Biosensors and Bioelectronics 126 (2019) 193–199

Contents lists available at ScienceDirect

Biosensors and Bioelectronics

journal homepage: www.elsevier.com/locate/bios

# Disposable stainless steel-based electrochemical microsensor for in vivo determination of indole-3-acetic acid in soybean seedlings

Haiyang Li[a,b], Cheng Wang[a], Xiaodong Wang[a], Peichen Hou[a], Bin Luo[a], Peng Song[a], Dayu Pan[a], Aixue Li[a,*], Liping Chen[a,*]

[a] Beijing Research Center of Intelligent Equipment for Agriculture, Beijing Academy of Agriculture and Forestry Sciences, Beijing 100097, China
[b] The State Key Laboratory of Biocontrol, School of Life Science, Sun Yat-sen University, Guangzhou 510060, China

ARTICLE INFO

*Keywords:*
IAA
Stainless steel
In vivo
Electrochemical sensor

ABSTRACT

In vivo detecting of plants signal molecules is of great importance for the precision farming, crop management and plant phenotyping. In this work, for in vivo detecting indole-3-acetic acid (IAA), one of phytohormones, fine stainless steel (SS) wire was used as electrode material. Highly ordered nanopores, popcorn-like Au nanostructures, Pt nanoparticles and reduced graphene oxide (ERGO) nanocomposite films, and polymerized ST film (PST) were fabricated on the SS microelectrode in turn for improving the detection effect. Using the as-prepared SS microelectrode as working electrode, two untreated SS wires as reference electrode and counter electrode respectively, a disposable electrochemical microsensor for IAA were developed. The microsensor exhibited excellent selectivity and high sensitivity with low detection limit (LOD) of 43 pg $mL^{-1}$. The limit of quantity (LOQ) is 143 pg $mL^{-1}$. The RSD was 7% for 12 different PST/Pt-ERGO/Au/a-SS microsensors in presence of 100 μg $mL^{-1}$ IAA. Using this microsensor, IAA of the stem of soybean seedlings was detected in vivo under salt stress. Our result was also confirmed by ultra-performance liquid chromatography-mass spectrum (UPLC-MS). This is the first report for the in vivo detection of IAA in plants using SS-based electrochemical microsensor. Our sensor provides an excellent sensing platform for detecting IAA in plants in vivo.

## 1. Introduction

Environmental conditions such as drought, freezing, heat and salt stress, etc, usually result in the activation of specific defense responses in plants (Ren et al., 2015). As signal molecules, phytohormones play an essential role in the regulatory processes of plants for stress adaptation. Indole-3-acetic acid (IAA) is an ubiquitous phytohormone. It participates in the regulation of various physiological processes which included in the growth, flowering, and withering of plants (Liu et al., 2007; Ma et al., 2008; Xi et al., 2009). It is also important in the response to salt stress for crop plants (Fahad et al., 2015).

Conventional methods for detecting IAA includes mass spectrometry analysis (MS) (Pollmann et al., 2002), liquid chromatography (LC) (Ren et al., 2013), spectrofluorometric method (Li et al., 2009), capillary electrophoresis (CE) (Chen et al., 2011), chemiluminescence (Xu et al., 2012), and radioimmunoassay (Madej and Häggblom, 1985), etc. But all these methods are in vitro methods. The plant samples, such as roots, stems and leaves, need to be pretreated. This procedure is complicated and time-consuming, and always results in the loss of some important biological information. Nowadays, more and more attention has been paid to develop in vivo methods for detecting signal molecules of plants, so as to obtain more instant and accurate information about the response mechanism of plants under different environmental conditions. Therefore, it is very necessary to develop in vivo methods for detecting IAA.

Electrochemical sensor has the characteristics of high sensitivity, good selectivity, simple operation, low cost, and easily to be miniaturized and integrated (Ali and Choudhry, 2015; Antilen et al., 2016; Bojdi et al., 2014a, 2014b, 2015, 2016; Hosseini et al., 2014; Fan et al., 2017; Sun et al., 2016; Wu et al., 2017). It is expected to become one of the better solutions for detecting signal molecules of plants in vivo. Researchers have developed some electrochemical sensors for detecting signal molecules of plants in vivo. For example, L.J. Sun et al. (2014) detected a phytohormone, salicylic acid (SA), in tomato leaves in vivo by a paper-based electrochemical sensor. Xu et al. (2009) monitored oxidative burst induced by ultraviolet A and ultraviolet C radiation in oilseed rape in vivo by a modified Pt microbiosensor. However, up to date, few electrochemical sensors have been reported for detecting IAA in plants in vivo.

Because of the complex environment of living bodies, microsensors

* Corresponding authors.
*E-mail addresses:* liax@nercita.org.cn (A. Li), chenlp@nercita.org.cn (L. Chen).

https://doi.org/10.1016/j.bios.2018.10.041
Received 8 August 2018; Received in revised form 15 October 2018; Accepted 22 October 2018
Available online 24 October 2018
0956-5663/ 

are easily to be fouled, thereby losing their activity and reducing their detection life. One of solutions for this problem is to develop disposable, low-cost microsensor. Stainless steel (SS) is a kind of alloy which possesses unique characteristics, including good electrical conductivity, high mechanical strength, biocompatibility, and low-cost, etc. It has been employed as an attractive substrate for many biomedical tools and devices (Pramatarova et al., 2007; Talha et al., 2013). Additionally, the manufacturing process for SS is mature, thus ensuring its stable performance. It has been used as inexpensive and disposable electrode material which showed a great potential application in biosensors (Guo et al., 2011; Ivnitski et al., 2000; Wu et al., 2000; Yang et al., 2010). Therefore, in this work, using fine SS wire as electrode material, highly ordered self-organized nanopores were firstly formed on the SS surface by electrochemical anodization process. Au nanostructures, Pt nanoparticles and reduced graphene oxide (ERGO) nanocomposite films were electrodeposited on the anodized SS electrode in turn for enhancing the catalytic effect. ST (Fig. S1) is a cationic dye. It has been reported that electro-polymerized ST film (PST) can strongly attract IAA and enhance the electrochemical response of IAA (Gan et al., 2011). So PST film was further fabricated on the SS microelectrode. Using the as-prepared SS microelectrode as working electrode, two untreated SS wires as reference electrode and counter electrode separately, we developed a disposable electrochemical microsensor for IAA. And IAA of the soybean seedlings under salt stress was detected in vivo by this microsensor. This is the first report for the in vivo detection of IAA in plants using SS-based electrochemical microsensor. Our result was also confirmed by UPLC-MS.

## 2. Experimental

### 2.1. Materials

Hexachloroplatinic acid hexahydrate ($H_2PtCl_6{\cdot}6H_2O$), safranine T (ST), indole-3-acetic acid (IAA), salicylic acid, citric acid, abscisic acid, succinic acid, and malic acid were obtained from Sigma. Gold chloride ($HAuCl_4{\cdot}4H_2O$) and monolayer graphene oxide (GO) (diameter: 500 nm to 5 μm) was obtained from XFNano Material Tech Co., Ltd. (Nanjing, China). All other chemicals were of analytical reagent grade.

### 2.2. Fabrication of the SS microsensor

The 304 stainless steel wire (SS, d = 0.25 mm, Alfa Aesar, China) was ultrasonically cleaned for 10 min in water and ethanol. After drying by $N_2$, it was anodized in 0.3 mol $L^{-1}$ $NaH_2PO_4$ solution at 30 V for 10 min at room temperature. A graphite rod (d = 0.5 cm) was used as the cathode. The prepared anodized SS wire (a-SS) was ultrasonically cleaned in water and dried by $N_2$. A glass capillary (o.d. 1.5 mm, length 100 mm) was pulled on a microelectrode puller (SUTTER P-97, USA) into two capillaries. The a-SS wire was carefully inserted into the capillary. About 2 mm of the anodized part of the SS wire was exposed from one end of the capillary and used as working electrode, and the other un-anodized part of SS was exposed from the other end of the capillary and used as conducting wire. Epoxy resin was used to seal both ends of the capillary. For the fabrication process, a Ag/AgCl electrode (saturated KCl) and a Pt wire (0.5 mm, diameter) were applied as reference electrode and counter electrode respectively.

After cleaning, the electrodeposition of Au nanoparticles on the prepared a-SS microelectrode was carried out in 50 mM $HAuCl_4$, 1.1 M $Na_2SO_3$, and 0.3 M $Na_2HPO_4$ solution under − 1 V by amperometric I-t method. Then the electrodeposition of Pt nanoparticles/ERGO nanocomposite films (Pt-ERGO) on the Au layer was carried out in 0.3 M NaAc solution containing 2 mg $mL^{-1}$ $H_2PtCl_6$ and 2 mg $mL^{-1}$ GO under the potential from −1.5 to 0 V by cyclic voltammogram. Finally, the PST film was fabricated by potential sweep in 0.5 mM ST (containing 0.1 M $H_2SO_4$ and 0.1 M $KNO_3$) from −0.80 to 1.60 V. The PST film modified electrode was denoted as PST/Pt-ERGO/Au/a-SS sensor.

### 2.3. Characterizations

SEM imaging and EDS analysis of the modified SS electrode was conducted on a FESEM system equipped with EDS microprobe (JEOL JSM-6700F). X-ray photoelectron spectroscopy (XPS) was taken on ESCALAB 250Xi photoelectron spectrometer (Thermo Fisher Scientific, Inc., USA) with Al Kα X-ray radiation as the X-ray source.

### 2.4. Preparation of plant materials

The soybean seeds (ZH13) were got from Beijing Kafry Technology Co., LTD. They were cultured in an incubation chamber at 14 h photoperiod and 25 ± 2 °C /18 ± 2 °C. After germination, the seedlings were cultured in Hoagland solution. They were randomly divided into eight groups when they grew to 15 days, each group contained 20 plants. Two levels of salts (0 and 100 mM) and 0, 12, 24 and 36 h of salt treatment were used for the salt stress experiment.

### 2.5. Electrochemical measurements

All the electrochemical experiments were carried out on PGSTAT302N AUTOLAB electrochemical analyzer system (Eco Chemie B. B. Netherlands). The modified PST/Pt-ERGO/Au/a-SS electrode was applied as working electrode, and two untreated SS wires were separately used as the reference electrode and the counter electrode. For each measurement, a different PST/Pt-ERGO/Au/a-SS sensor was used.

For in vivo measurement of IAA, three holes were obtained in the stem of the soybean seedlings by a puncture needle. The working electrode, reference electrode and the counter electrode were separately placed into the holes. The electrodes was placed approximately the same site for different plant. During the insertion process, special attention was paid to avoid any touch of the microsensor to the plant tissue, so as to maintain the integrity of the microsensor.

### 2.6. Detection of IAA by ultra-performance liquid chromatography-mass spectrum (UPLC-MS)

The stem samples of the soybean seedlings were collected to extract for IAA for UPLC-MS analysis (Water Acquity I-Class, US; Thermo Q-Exactive, US) according to previous report (Li et al., 2017). Briefly, liquid nitrogen was used to grind the samples. The ground power (100 mg) was extracted overnight at 4 °C after adding 1 mL 4 °C pre-cooled methanol. After adding 1 mL of $CHCl_3$, the solution was vortexed and shaked (900 rpm, 4 min). Then, the underlying liquid was collected after centrifuging at 12,000 rpm for 5 min. Finally, 1 mL of methanol was added into the sample. After passing through microporous membrane (0.22 μm), UPLC-MS was performed using the prepared samples.

## 3. Results and discussion

### 3.1. Choice of electrode materials

In this work, a disposable electrochemical microsensor for IAA based on SS was developed as shown in Scheme 1. SS was used as the base electrode due to its unique characteristics, including good electrical conductivity, high mechanical strength, biocompatibility, high stability and low-cost. It has been shown great potential in sensor construction. For example, Guo et al. developed a glucose biosensor by modifying SS with chitosan-glucose oxidase biocomposite and Pt–Pb nanoparticles (Guo et al., 2011). Rezaei et al. (2013) developed a disposable immunosensor for doxorubicin based on an aminosilane layer and gold nanoparticles modified SS substrate. Compared with smooth surface, nanostructured surface can enhance the surface area of electrode, thus enhancing the conductivity of the electrode. So we formed highly ordered nanopores on the SS surfaces by electrochemical anodization process. The anodized SS electrode is denoted as a-SS. Au

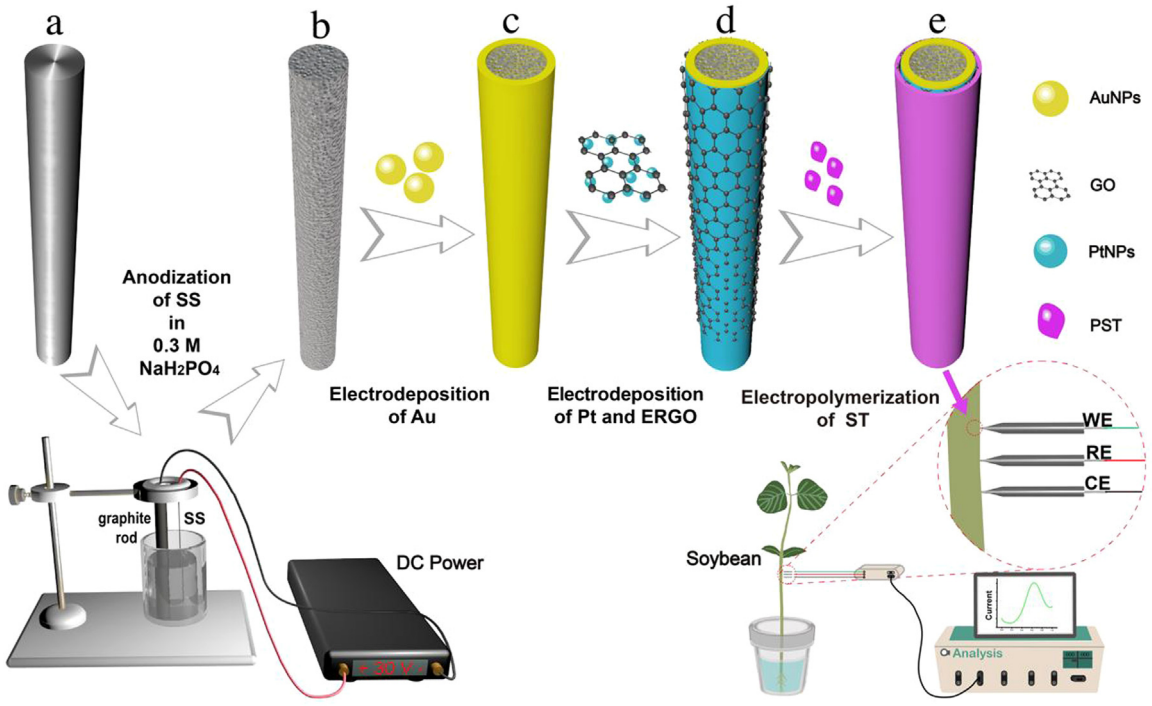


**Scheme 1.** The schematic illustration of the fabrication process of the SS microelectrode: bare SS (a), a-SS (b), Au/a-SS (c), Pt-ERGO/Au/a-SS (d), PST/Pt-ERGO/Au/a-SS (e).

nanostructures have good electrical conductivity and biocompatibility, it has been extensively used in the fabrication of sensor to increase its conductivity (Chen et al., 2015). So Au nanostructures were further electrodeposited on the anodized SS surface (Au/a-SS). Pt nanostructures and reduced graphene oxide (ERGO) are two commonly used materials for enhancing conductivity and catalytic activity of sensors. Pt-ERGO nanocomposite films can be obtained by direct co-electrodeposition method. It has been reported that the prepared Pt-ERGO nanocomposite films can exhibit excellent catalytic activity (Yang et al., 2011; Zhu et al., 2012). So we choose to form the Pt-ERGO nanocomposite films on the Au/a-SS electrode by co-electrodeposition method (Pt-ERGO/Au/a-SS). ST is a kind of cationic dye. Its chemical formula is shown in Fig. S1. Gan et al. reported that electro-polymerized PST film can strongly attract IAA and enhance the electrochemical response of IAA (Gan et al., 2011). So PST film was further fabricated on the Pt-ERGO/Au/a-SS microelectrode. This electrode was denoted as PST/Pt-ERGO/Au/a-SS.

### 3.2. Characterization of the modified electrode

The morphology of electrode was characterized by SEM. As shown in Fig. 1, the surface of bare SS electrode is smooth and clean (Fig. 1A). After electrochemical anodization, nanoporous honeycomb structure appears on the electrode surface with the nanopores size of 100–500 nm (Fig. 1B). Electrodeposition method was used to deposit Au nanoparticles on the a-SS. The deposition potential and time were optimized (Fig. S2A). When − 1.0 V, 100 s was used, the optimal electrochemical performance of the sensor for IAA was obtained. Electrodeposition of Au nanoparticles on the anodized SS surface leads to nearly hemispherical-shaped Au nanoparticles, and some polyhedral Au nanoparticles appear and form “popcorn-like” nanoclusters (Fig. 1C). The diameter of Au nanostructures is about 200–800 nm. Then, Pt nanoparticles and ERGO were simultaneously electro-deposition and electroreduction on the Au/a-SS surface by cyclic voltammetry (CV) method. The optimal electrochemical performance was obtained under − 1.5 V to 0 V, 10 circles (Fig. S2B). As shown in Fig. 1D, Pt nanoparticles covered by lamellar ERGO can be observed. PST can be formed by a simple electropolymerization method (Gan et al., 2011). The best performance for the electropolymerization was obtained at 10 circles (Fig. S2C). The electropolymerization of ST produces aggregated ST particles on the electrode surface (Fig. 1E), which make a rougher surface.

The element composition for the modified electrode was characterized by EDS technique. EDS of the bare SS shows the main elements of SS, including Fe, Mn, Cr, C, Ni (Fig. 1a). For the a-SS, the EDS spectrum is basically consistent with that before anodization. The appearance of O element indicates the anodization effect (Fig. 1b). EDS of the Au/a-SS electrode shows the appearance of Au element, and the appearance of Na might be ascribed to the application of solutions containing $Na^+$ during the deposition process of Au nanoparticles (Fig. 1c). Pt element appears for the EDS spectrum of the Pt-ERGO/Au/a-SS electrode (Fig. 1d), and atomic% for the C (53.01) and O (29.37) increase compared to those of (C: 40.12, O: 22.78) in Fig. 1c, confirming the deposition of Pt nanoparticles and ERGO. As expected, EDS spectrum of the PST/Pt-ERGO/Au/a-SS electrode shows the appearance of N, Cl atoms (Fig. 1e), which is contained in the PST molecules. The EDS results confirm the successful fabrication of the electrode.

Fig. S3 shows X-ray photoelectron spectroscopy (XPS) characterization of the modification processes. As shown in Fig. S3A, there was a small peak of O1s at 530.3 eV for the bare SS electrode. The intensity of O1s peak increased (a-SS) indicating oxidation reaction occurs during the electrochemical anodization process. Au 4f7/2 (83.8 eV) and Au 4f5/2 (87.7 eV) were clearly observed in Fig. S3B, indicating the successful electrodeposition of Au particles on the a-SS (Au/ a-SS). There was a small peak of C1s at 285.0 eV for the Au/a-SS electrode (Fig. S3C), as the main elements of SS included C element. For the Pt-ERGO/Au/a-SS electrode, the C1s peak increased obviously, and Pt 4f7/2 (71.0 eV) and Pt 4f5/2 (74.4 eV) appeared, indicating the successfully modification of Pt nanostructures and ERGO on the Au/a-SS electrode. PST molecules contained Cl element (Fig. S1), so Cl 2p (198.8 eV) was clearly observed after electro-polymerized PST film on the Pt-ERGO/Au/a-SS electrode (Fig. S3D). The XPS result also confirmed the successful fabrication of the electrode.

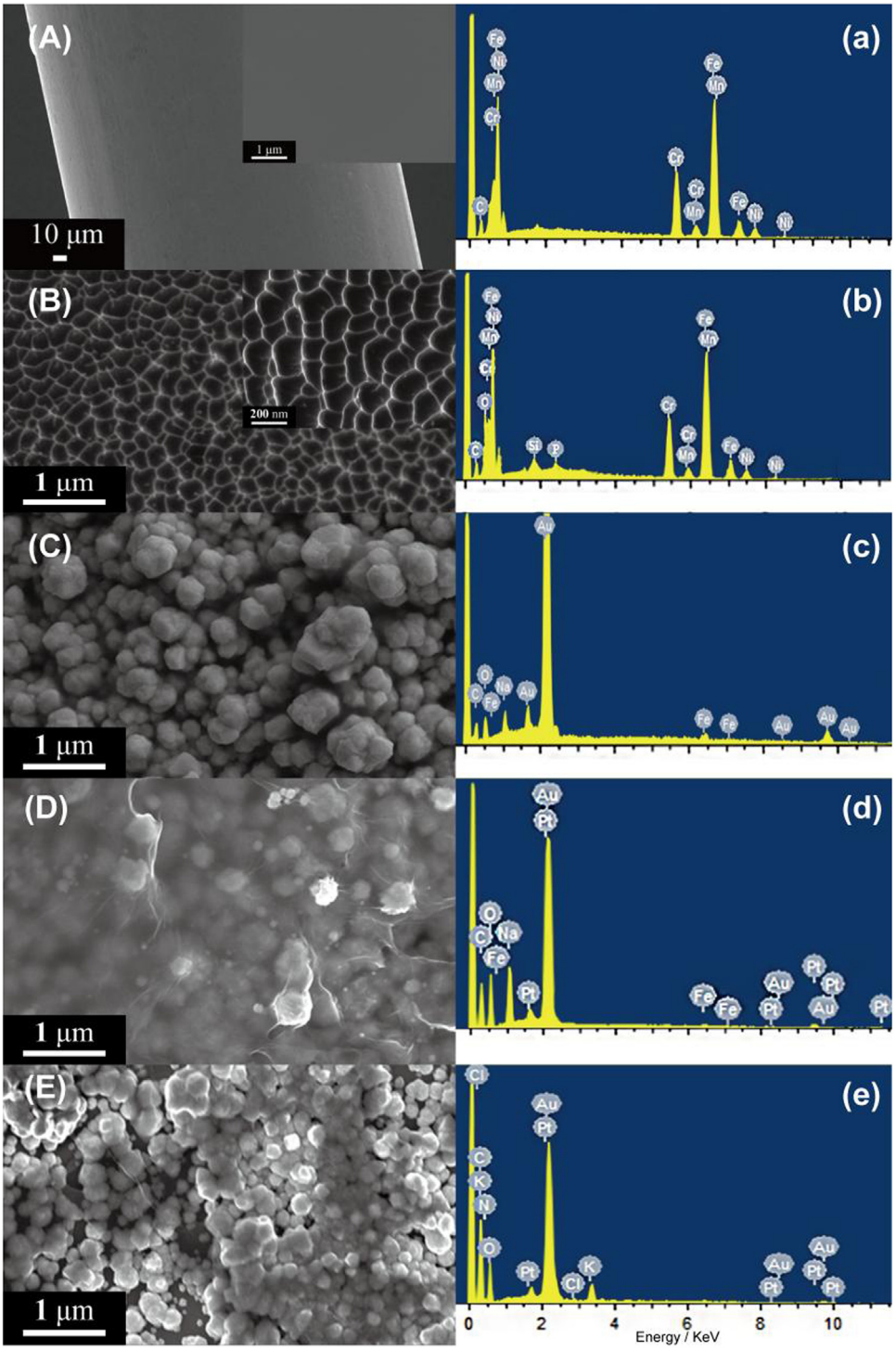


**Fig. 1.** SEM (A-E) and EDS (a-e) spectrum analysis of bare SS, a-SS, Au/a-SS, Pt-ERGO/Au/a-SS and PST/Pt-ERGO/Au/a-SS.

The effective surface area of the different modified SS electrodes was evaluated based on Randles–Sevcik equation. The experiment was performed in $5 \times 10^{-3}$ M $K_3[Fe(CN)_6]$ solution at various scan rates (Fig. S4). For a reversible process, the following equation can be utilized (Luo et al., 2014; Xu et al., 2014):

$$I_p = 2.69 \times 10^5 \times (D_0) \cdot A \cdot v^{1/2} \cdot n^{3/2} \cdot C_0$$

Where $D_0$ is the diffusion coefficient of the molecule in solution ($cm^2\ s^{-1}$), A is the effective area of the electrode ($cm^2$), $v$ is the scan rate ($V\ s^{-1}$), n is the number of electrons including in the redox reaction, and $C_0$ is the concentration of the probe in the solution ($mol\ cm^{-3}$). For $[Fe(CN)_6]^{3-}/[Fe(CN)_6]^{4-}$, $n = 1$, $C_0 = 5 \times 10^{-6}$ $mol\ cm^{-3}$, $D_0 = 1 \times 10^{-5}$ $cm^2\ s^{-1}$ (Wang et al., 2012). The effective surface area were 0.047 $cm^2$, 0.076 $cm^2$, 0.184 $cm^2$, and 0.256 $cm^2$ for the a-SS, Au/a-SS, Pt-ERGO/Au/a-SS, and PST/Pt-ERGO/Au/a-SS respectively, which was much higher than that of bare SS (0.016 $cm^2$).

### 3.3. Feasibility of the PST/Pt-ERGO/Au/a-SS microelectrode for detecting IAA

The feasibility of the PST/Pt-ERGO/Au/a-SS microelectrode for detecting IAA was evaluated by CV and differential pulse

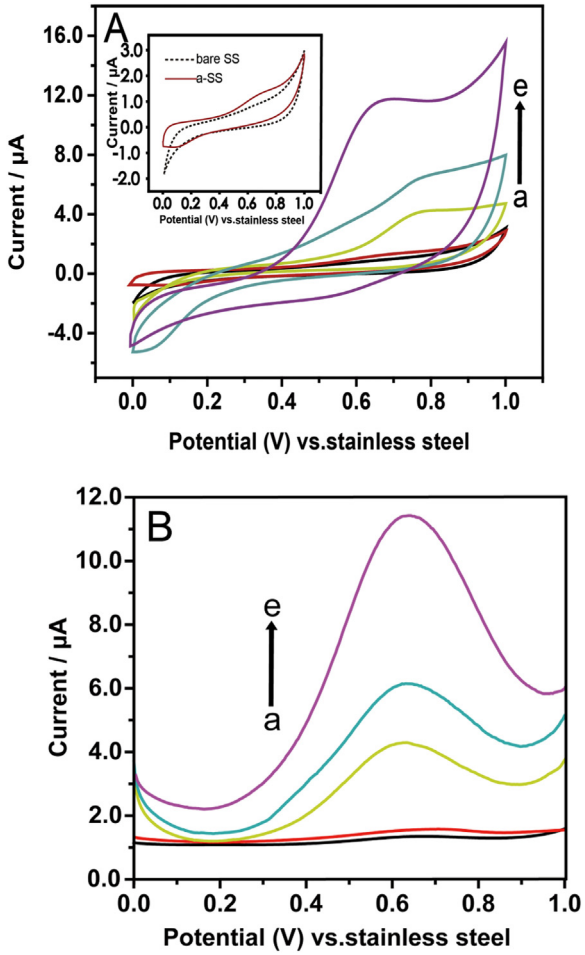


**Fig. 2.** CV (A) and DPV (B) characterization of bare SS (a), a-SS (b), Au/a-SS (c), Pt-ERGO/Au/a-SS (d), PST/Pt-ERGO/Au/a-SS (e) in 0.01 M PBS (pH 7.4) containing 100 μg $mL^{-1}$ IAA.

voltammograms (DPV) techniques. In the presence of 100 μg $mL^{-1}$ IAA, there are no obvious oxidation peak in the CV curve (Fig. 2A) for the bare SS (curve a). After anodization, a weak oxidation peak for IAA appears near 0.7 V (curve b), indicating that the anodization process effectively increases the surface area and amount of active site of the SS microelectrode. After electrodeposition of Au nanoparticles (curve c) and Pt-ERGO composite film (curve d) in turn, the surface area and the electronic transfer capability of the microelectrode increase due to the excellent electrical conductivity and superior catalytic activity of Au nanoparticles, Pt nanoparticles and ERGO. So the electrochemical response of IAA is enhanced with the layer by layer modification. After electropolymerization of ST (curve e), the electrochemical response of IAA is further enhanced because of the strongly attraction effect of positive-charged PST film (with plenty amido) to IAA.

The DPV curves of IAA at different modified SS microelectrodes were shown in Fig. 2B. As expected, the oxidation peak of IAA on the SS (curve a) and a-SS (curve b) electrode are very weak. The oxidation peak of IAA appears near at 0.7 V after electrodeposition of Au NP (curve c). And it becomes more obvious with the layer by layer modification process. The biggest peak current is obtained after the polymerization of ST on the electrode. The DPV result is consistent with that of CV. The results of CV and DPV confirm that the PST/Pt-ERGO/Au/a-SS microelectrode can be used for detecting IAA.

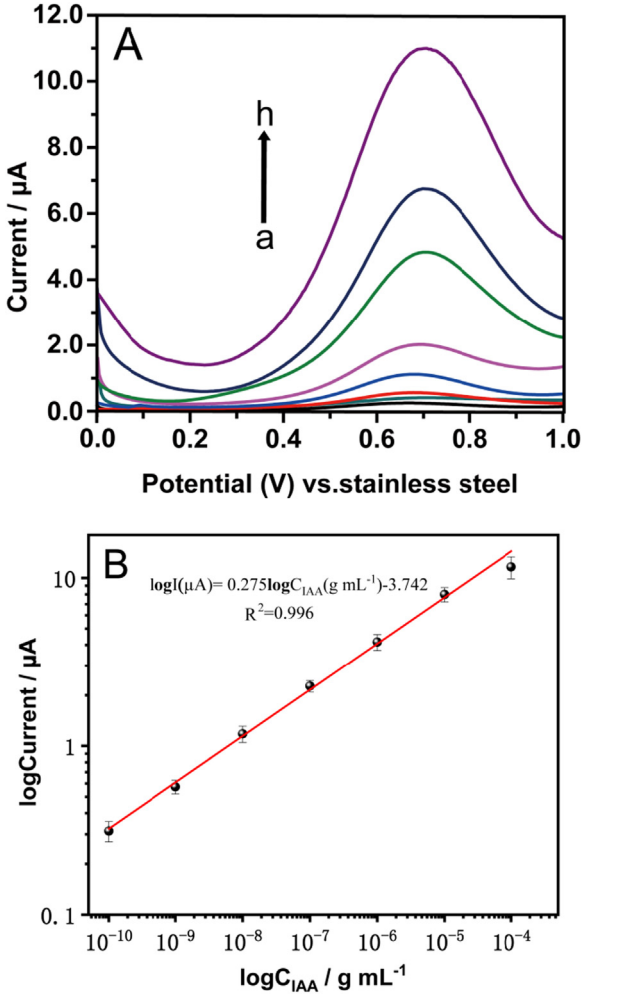


**Fig. 3.** (A) DPV plot for IAA of various concentrations at PST/Pt-ERGO/Au/a-SS microelectrode: (a) 0, (b) 100 pg $mL^{-1}$, (c) 1 ng $mL^{-1}$, (d) 10 ng $mL^{-1}$, (e) 100 ng $mL^{-1}$, (f) 1 μg $mL^{-1}$, (g) 10 μg $mL^{-1}$, (h) 100 μg $mL^{-1}$. (B) Calibration curve of PST/Pt-ERGO/Au/a-SS microsensor for IAA.

### *3.4. Performance of the PST/Pt-ERGO/Au/a-SS microelectrode for detecting IAA*

The quantitative determination of IAA was carried out by DPV. Fig. 3A shows the DPV responses of the PST/Pt-ERGO/Au/a-SS microelectrode towards different concentrations of IAA in 0.01 M PBS buffer (pH 7.4). With the increasing concentrations of IAA, the DPV responses of the PST/Pt-ERGO/Au/a-SS microelectrode increase correspondingly. The logarithmic value of the peak current is linearly related to the logarithmic value of the IAA concentration from 100 pg $mL^{-1}$ to 100 μg $mL^{-1}$ (Fig. 3B). The linear regression equation is expressed as log I(μA) = 0.275log$C_{IAA}$(g $mL^{-1}$)-3.742, and the correlation coefficent is 0.996. The estimated LOD and LOQ of the modified sensor are 43 pg $mL^{-1}$ and 143 pg $mL^{-1}$, which are calculated from 3σ/m and 10σ/m, respectively (σ: standard deviation of the blank response, m: slope of the calibration curve). The LOD and linear range of the IAA microsensor is comparable to or better than some IAA sensors previous reported as shown in Table 1.

The selectivity of the sensor is evaluated in presence of potential interferences. As shown in Fig. 4, the characteristic peak of IAA appeared at 0.7 V, while the characteristic peak of other interferences, including malic acid, abscisic acid, salicylic acid, citric acid, and succinic acid, appeared respectively at 0.83 V, 0.88 V, 1.0 V, 1.12 V, and 1.22 V. The potentials of these interferences are more negative than that

**Table 1**
Comparisons of the proposed IAA sensor with the previous reported IAA sensors.

| Electrode | Method | Linear range (ng mL$^{-1}$) | LOD (ng mL$^{-1}$) | References |
|---|---|---|---|---|
| Carbon tape modified electrode | DPV | 175– 17,500 | 17.5 | (L.J. Sun et al., 2018) |
| MWCNTs-Chitosan/GCE | DPV | 117.3–8543.5 | 17.5 | (Sun et al., 2015) |
| SiO2@AuNPs | DPV | 35–9625 | 9.08 | (J. Sun et al., 2018) |
| hemin/rGO/GCE | I-T | 17.5–7525 | 12.95 | (Liu et al., 2016) |
| MWCNTs/SDC/GCE | DPV | 17.5–5250 | 5.18 | (Lu et al., 2016) |
| CTAB/MPTS/Mt/GCE | DPV | 1.75– 140,000 | 0.35 | (Yang, 2016) |
| Ab-MPA-CdS/RGO/ITO | Photocurrent | 0.1–1000 | 0.05 | (B. Sun et al., 2014) |
| PST/Pt-ERGO/Au/a-SS | DPV | 0.1– 100,000 | 0.043 | This work |

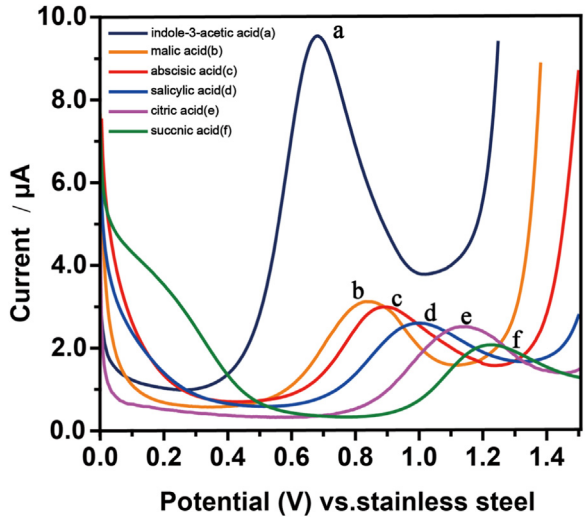


**Fig. 4.** DPV plot of PST/Pt-ERGO/Au/a-SS microsensor to abscisic acid, succinic acid, citric acid, malic acid, salicylic acid and IAA. The concentration of IAA was 100 μg mL$^{-1}$.

of IAA. And peak current of the interferences was much lower than that of IAA when same concentrations were tested (100 μg mL$^{-1}$). The result showed that the developed IAA microsensor has good selectivity. The RSD was 7% for 12 different PST/Pt-ERGO/Au/a-SS microsensors in presence of 100 μg mL$^{-1}$ IAA. After storage at 4 °C for three weeks, 87% sensing ability remained for the microsensor, which indicated that this microsensor is highly stable.

### 3.5. In vivo determination of IAA in soybean seedlings

The prepared microsensor was used to monitor the change of IAA level in the stem of soybean seedlings under salt stress in vivo (Table 2). The photograph for the in vivo detection of IAA is shown in Fig. S5. For the control groups, during the 36 h treatment, the IAA level fluctuates slightly around 50–70 ng mL$^{-1}$. For the salt-treated groups, the IAA level rise to 157.44 ± 23.03 ng mL$^{-1}$ after 12 h salt treatment, at which point the IAA concentration in stems of soybean is about two times as that of the control groups. After 24 h salt treatment, the IAA declines to a low level, i.e. 10.55 ± 2.84 ng mL$^{-1}$. After 36 h salt treatment, the IAA level declines further. The result of UPLC-MS shows similar trend with those obtained by the proposed electrochemical sensor (Fig. S6), which confirms that the developed microsensor is reliable for detecting IAA in vivo. In comparison to conventional techniques, the information obtained from our proposed microsensor most probably reflects those in vivo situations. And our proposed microsensor is simple, rapid, portable and disposable, which has the potential for field application. And the influences on the plants can be neglected as the diameter of the microelectrode is only 0.25 mm.

IAA is an important phytohormone which plays a major role on regulating plant growth. It also responds to salinity in crop plants (Akbari et al., 2007; Javid et al., 2011). Our results show that the IAA level is raised first and then declined during the 36 h salt-treatment. The mechanism for this phenomenon is not very clear. IAA patterns are strongly depended on its transport. One of the important IAA transporters was PIN2 (van den Berg et al., 2016). van den Berg et al. (2016) found a reduction of PIN2 on the salt-exposed side of the *Arabidopsis* root, which leads to the accumulation of IAA in the meristem. The detected position in our work was the top of the soybean stems, belonging to one kind of meristem. This may be one of the reasons for the initial rise of IAA level. Schopfer et al. (2002) reported that IAA could enhance drought tolerance by modulating ABA-responsive gene expression and ROS metabolism, implying that IAA play some roles in improving the tolerance abilities of plants to environment stresses. So the rising of IAA may also be due to a self-regulation of plants in presence of salt stress. However, after a long time of salt treatment, the IAA level declined because of the damage of salt stress on the plants. Naser et al. also believed that IAA-mediated growth inhibition is one of strategies of plants to adapt to the environment stresses (Naser and Shani, 2016). Similar trends were also observed for the IAA levels of heat-treated soybean (Zi-Xian et al., 1999) and salt-treated Jerusalem artichoke (Shao et al., 2016). Our results indicate that IAA signaling has an important role in the response to salt stress in soybean. The exact mechanism for this phenomenon will be investigated further.

## 4. Conclusion

In summary, an IAA sensor was proposed by fabrication of gold nanostructures, Pt nanoparticles and ERGO nanocomposite film, and PST film on anodized SS microelectrode simply with electrochemical methods. The proposed IAA sensor showed high sensitivity and selectivity. It is simple, rapid, portable and disposable, which has the

**Table 2**
Comparison of the results obtained by UPLC-MS and the developed microsensor for detecting IAA in the stem of soybean seedlings under salt stress.

| Time (h) | Control | | | Salt Stress | | |
|---|---|---|---|---|---|---|
| | UPLC-MS (ng mL$^{-1}$) | Sensor (ng mL$^{-1}$) | Relative deviation (%) | UPLC-MS (ng mL$^{-1}$) | Sensor (ng mL$^{-1}$) | Relative deviation (%) |
| 0 | 63.03 ± 6.47 | 65.82 ± 4.74 | 4.24 | 63.03 ± 6.47 | 65.82 ± 4.74 | 4.24 |
| 12 | 67.65 ± 6.72 | 70.03 ± 6.56 | 3.40 | 142.74 ± 16.33 | 157.44 ± 23.03 | 9.34 |
| 24 | 66.18 ± 8.69 | 72.30 ± 5.85 | 8.65 | 9.25 ± 3.37 | 10.55 ± 2.84 | 3.24 |
| 36 | 61.89 ± 6.11 | 68.52 ± 5.78 | 9.68 | 6.13 ± 1.71 | 5.88 ± 1.85 | − 4.08 |

potential for field application. And it is used for in vivo detection of the IAA concentrations of the soybean seedlings under salt stress. The proposed sensor would be of great value for monitoring plant physiological state in vivo. Future work may include further optimizing of the microsensor, developing integrated sensing system, and expanding its applications to monitor various physiological states of plants in vivo.

## Acknowledgements

The authors are thankful for the fundings from Beijing Natural Science Foundation (2182022), Scientific and Technological Innovation Team of Beijing Academy of Agricultural and Forestry Sciences (JNKYT201604), and National Natural Science Foundation of China (Grant No. 61571443).

## Appendix A. Supplementary material

Supplementary data associated with this article can be found in the online version at doi:10.1016/j.bios.2018.10.041.

## References

Akbari, G., Sanavy, S.A., Yousefzadeh, S., 2007. Pak. J. Biol. Sci. 10, 2557–2561.
Ali, M., Choudhry, M.A., 2015. Mater. Sci. Pol. 33, 213–219.
Antilen, M., Bustos, O., Ramirez, G., Canales, C., Faundez, M., Escudey, M., Pizarro, C., 2016. New J. Chem. 40, 7132–7139.
Bojdi, M.K., Behbahani, M., Sahragard, A., Amin, B.G., Fakhari, A., Bagheri, A., 2014a. Electrochim. Acta 149, 108–116.
Bojdi, M.K., Mashhadizadeh, M.H., Behbahani, M., Farahani, A., Davarani, S.S.H., Bagheri, A., 2014b. Electrochim. Acta 136, 59–65.
Bojdi, M.K., Behbahani, M., Najafi, M., Bagheri, A., Omidi, F., Salimi, S., 2015. Electroanalysis 27, 2458–2467.
Bojdi, M.K., Behbahani, M., Hesam, G., Mashhadizadeh, M.H., 2016. RSC Adv. 6, 32374–32380.
Chen, D., Wang, C., Chen, W., Chen, Y., Zhang, J.X.J., 2015. Biosens. Bioelectron. 74, 1047–1052.
Chen, H., Guo, X.F., Zhang, H.S., Wang, H., 2011. J. Chromatogr. B 879, 1802–1808.
Fahad, S., Hussain, S., Matloob, A., Khan, F.A., Khaliq, A., Saud, S., Hassan, S., Shan, D., Khan, F., Ullah, N., 2015. Plant Growth Regul. 75, 391–404.
Fan, J., Qi, K., Zhang, L., Zhang, H., Yu, S., Cui, X., 2017. ACS Appl. Mater. Interfaces 9, 18008–18014.
Gan, T., Hu, C., Chen, Z., Hu, S., 2011. Talanta 85, 310–316.
Guo, M., Fang, H., Wang, R., Yang, Z., Xu, X., 2011. J. Mater. Sci. Mater. Med. 22, 1985–1992.
Hosseini, H., Behbahani, M., Mahyari, M., Kazerooni, H., Bagheri, A., Shaabani, A., 2014. Biosens. Bioelectron. 59, 412–417.
Ivnitski, D., Wilkins, E., Tien, H.T., Ottova, A., 2000. Electrochem. Commun. 2, 457–460.
Javid, M.G., Sorooshzadeh, A., Moradi, F., Sanavy, S.A.M.M., Allahdadi, I., 2011. Aust. J. Crop Sci. 5, 726–734.
Li, H., Hu, Y., Li, A., Wang, X., Hou, P., Wang, C., Chen, K., Zhao, C., 2017. RSC Adv. 7, 54416–54421.
Li, Y.N., Wu, H.L., Zhu, S.H., Nie, J.F., Yu, Y.J., Wang, X.M., Yu, R.Q., 2009. Anal. Sci. Int. J. Jpn. Soc. Anal. Chem. 25, 83–88.
Liu, F., Tang, J., Xu, J., Shu, Y., Xu, Q., Wang, H., Hu, X., 2016. Biosens. Bioelectron. 86, 871–878.
Liu, H.T., Li, Y.F., Luan, T.G., Lan, C.Y., Shu, W.S., 2007. Chromatographia 66, 515–520.
Lu, L., Yu, Y., Zhou, H., Li, P., Peng, Y., Wang, W., He, H., 2016. Int. J. Electrochem. Sci. 11, 2392–2400.
Luo, S., Xiao, H., Yang, S., Liu, C., Liang, J., Tang, Y., 2014. Sens. Actuators B: Chem. 194, 325–331.
Ma, W., et al., 2008. Anal. Chim. Acta 610, 274–281.
Madej, A., Häggblom, 1985. Physiol. Plant. 64, 389–392.
Naser, V., Shani, E., 2016. Plant Mol. Biol. 91, 661–672.
Pollmann, S., Mā¼Ller, A., Piotrowski, M., Weiler, E.W., 2002. Planta 216, 155–161.
Pramatarova, L., Pecheva, E., Krastev, V., 2007. J. Mater. Sci. Mater. Med. 18, 441–447.
Ren, Q.Q., Huang, X.R., Liu, G.C., Ou-Yang, J., Li, M.T., Chen, H., Zhao, Y., Di, Chen, W., 2015. Sens. Actuators B Chem. 220, 743–748.
Ren, Y., Deng, H., Shen, W., Gao, Z., 2013. Anal. Chem. 85, 4784–4789.
Rezaei, B., Havakeshian, E., Ensafi, A.A., 2013. Biosens. Bioelectron. 48, 61–66.
Schopfer, P., Liszkay, A., Bechtold, M., Frahry, M., Wagner, A., 2002. Planta 214, 821–828.
Shao, T., Li, L., Wu, Y., Chen, M., Long, X., Shao, H., Liu, Z., Rengel, Z., 2016. Sci. Total Environ. 568, 891–898.
Sun, B., Chen, L., Xu, Y., Liu, M., Yin, H., Ai, S., 2014. Biosens. Bioelectron. 51, 164–169.
Sun, J., Gan, T., Zhai, R., Fu, W., Zhang, M., 2018. Ionics (Kiel). 24, 2465–2472.
Sun, J., Wang, B., Xue, Z., Li, Z.J., Yang, X., 2016. Anal. Chem. 88, 1355–1361.
Sun, L.J., Feng, Q.M., Yan, Y.F., Pan, Z.Q., Li, X.H., Song, F.M., Yang, H., Xu, J.J., Bao, N., Gu, H.Y., 2014. Biosens. Bioelectron. 60, 154–160.
Sun, L.J., Liu, X., Gao, L., Lu, Y., Li, Y., Pan, Z., Bao, N., Gu, H., 2015. Anal. Lett. 48, 1578–1592.
Sun, L.J., Zhou, J.J., Pan, J.L., Liang, Y.Y., Fang, Z.J., Xie, Y., Yang, H., Gu, H.Y., Bao, N., 2018. Sens. Actuators B Chem. 276, 545–551.
Talha, M., Behera, C.K., Sinha, O.P., 2013. Mater. Sci. Eng. C. Mater. Biol. Appl. 33, 3563–3575.
van den Berg, T., Korver, R.A., Testerink, C., Ten Tusscher, K.H.W.J., 2016. Development 143, 3350–3362.
Wang, C., Yuan, R., Chai, Y., Chen, S., Zhang, Y., Hu, F., Zhang, M., 2012. Electrochim. Acta 62, 109–115.
Wu, F., Su, L., Yu, P., Mao, L., 2017. J. Am. Chem. Soc. 139, 1565–1574.
Wu, M., Lin, Z., Li, Y., Ren, S., 2000. Sens. Actuators B Chem. 66, 269–271.
Xi, Z., Zhang, Z., Sun, Y., Shi, Z., Tian, W., 2009. Talanta 79, 216–221.
Xu, F., Wang, F., Yang, D., Gao, Y., Li, H., 2014. Mater. Sci. Eng.: C 38, 292–298.
Xu, H., Mei, Z., Wang, Z., He, Y., 2012. Spectrochim. Acta Part A Mol. Biomol. Spectrosc. 95, 114–119.
Xu, Q., Wei, F., Wang, Z., Yang, Q., Zhao, Y., Di, Chen, H., 2009. Sens. Actuators B Chem. 141, 599–603.
Yang, J., Tian, C., Wang, L., Fu, H., 2011. J. Mater. Chem. 21, 3384–3390.
Yang, Q., Atanasov, P., Wilkins, E., 2010. Electroanalysis 9, 1252–1256.
Yang, Y.J., 2016. Sens. Lett. 14, 756–763.
Zhu, M., Chen, P., Liu, M., 2012. Langmuir 28, 3385–3390.
Zi-Xian, L.U., Hong-Yi, F.U., Deng, X.D., Zhu, B.G., Liu, G.Q., Chen, J.N., 1999. J. Dev. Reprod. Biol. 8, 83–90.